Published in final edited form as:

Adv Mater. 2016 May ; 28(17): 3313–3320. doi:10.1002/adma.201505869.

Light-Activated Hypoxia-Responsive Nanocarriers for Enhanced Anticancer Therapy

Chenggen Qian,
Joint Department of Biomedical Engineering, University of North Carolina at Chapel Hill and North Carolina State University, Raleigh, NC 27695, USA

Division of Molecular Pharmaceutics and Center for Nanotechnology in Drug Delivery, Eshelman School of Pharmacy, University of North Carolina at Chapel Hill, Chapel Hill, NC 27599, USA

Department of Polymer Science & Engineering and Key Laboratory of High Performance, Polymer Materials & Technology of MOE, School of Chemistry & Chemical Engineering, Nanjing University, Nanjing, 210023, China

Jicheng Yu,
Joint Department of Biomedical Engineering, University of North Carolina at Chapel Hill and North Carolina State University, Raleigh, NC 27695, USA

Division of Molecular Pharmaceutics and Center for Nanotechnology in Drug Delivery, Eshelman School of Pharmacy, University of North Carolina at Chapel Hill, Chapel Hill, NC 27599, USA

Yulei Chen,
Department of Polymer Science & Engineering and Key Laboratory of High Performance, Polymer Materials & Technology of MOE, School of Chemistry & Chemical Engineering, Nanjing University, Nanjing, 210023, China

Quanyin Hu,
Joint Department of Biomedical Engineering, University of North Carolina at Chapel Hill and North Carolina State University, Raleigh, NC 27695, USA

Division of Molecular Pharmaceutics and Center for Nanotechnology in Drug Delivery, Eshelman School of Pharmacy, University of North Carolina at Chapel Hill, Chapel Hill, NC 27599, USA

Xuanzhong Xiao,
Department of Polymer Science & Engineering and Key Laboratory of High Performance, Polymer Materials & Technology of MOE, School of Chemistry & Chemical Engineering, Nanjing University, Nanjing, 210023, China

Wujin Sun,
Joint Department of Biomedical Engineering, University of North Carolina at Chapel Hill and North Carolina State University, Raleigh, NC 27695, USA

* zgu@email.unc.edu, qdshen@nju.edu.cn.

Supporting Information

Supporting Information is available from the Wiley Online Library or from the author.

Division of Molecular Pharmaceutics and Center for Nanotechnology in Drug Delivery, Eshelman School of Pharmacy, University of North Carolina at Chapel Hill, Chapel Hill, NC 27599, USA

Dr. Chao Wang,
Joint Department of Biomedical Engineering, University of North Carolina at Chapel Hill and North Carolina State University, Raleigh, NC 27695, USA

Division of Molecular Pharmaceutics and Center for Nanotechnology in Drug Delivery, Eshelman School of Pharmacy, University of North Carolina at Chapel Hill, Chapel Hill, NC 27599, USA

Peijian Feng,
Department of Polymer Science & Engineering and Key Laboratory of High Performance, Polymer Materials & Technology of MOE, School of Chemistry & Chemical Engineering, Nanjing University, Nanjing, 210023, China

Prof. Qun-Dong Shen*, and
Department of Polymer Science & Engineering and Key Laboratory of High Performance, Polymer Materials & Technology of MOE, School of Chemistry & Chemical Engineering, Nanjing University, Nanjing, 210023, China

Prof. Zhen Gu*
Joint Department of Biomedical Engineering, University of North Carolina at Chapel Hill and North Carolina State University, Raleigh, NC 27695, USA

Division of Molecular Pharmaceutics and Center for Nanotechnology in Drug Delivery, Eshelman School of Pharmacy, University of North Carolina at Chapel Hill, Chapel Hill, NC 27599, USA

Department of Medicine, University of North Carolina School of Medicine, Chapel Hill, NC 27599, USA

Graphical Abstract

A light-activated hypoxia-responsive conjugated polymer-based nanocarrier is developed for efficiently producing singlet oxygen ($^1O_2$) and inducing hypoxia to promote release of its cargoes in tumor cells, leading to enhanced antitumor efficacy. This dual-responsive nanocarrier provides an innovative design guideline for enhancing traditional photodynamic therapeutic efficacy integrated with a controlled drug release modality.

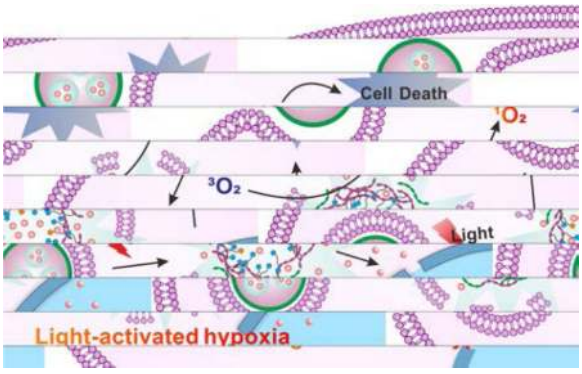

Keywords

drug delivery; nanomedicine; photodynamic therapy; hypoxia-responsive; conjugated polymer

Photodynamic therapy (PDT), as an important non-invasive therapeutic modality, has been clinically approved for cancer treatment.[1] PDT depends on the ability of photosensitizers to transfer energy from light to the surrounding molecular oxygen ($^3O_2$) to generate cytotoxic reactive oxygen species (ROS), especially singlet oxygen ($^1O_2$), resulting in the destruction of cells and tumor blood vessels.[2] PDT has particular advantages over other conventional therapies, in terms of its minimally invasive nature, tolerance of repeated doses, and fast healing process.[3] However, the limited water-solubility and tumor selectivity of most photosensitizers affect PDT efficacy and may induce the phototoxicity to adjacent normal tissues. To further enhance PDT's potency, polymer-photosensitizer conjugates or photosensitizer-loaded nanoparticles[4], such as polyplex micelles[5], gold nanoparticles[6], upconverting nanoparticles[7], carbon dots[8], and mesoporous silica nanoparticles[9] are utilized to optimize the tumor accumulation of therapeutics.

During the conversion of molecular oxygen ($^3O_2$) to singlet oxygen ($^1O_2$), the continuous oxygen consumption[10] and vascular shutdown effects[11] facilitate generation of hypoxic condition. In light of this, integration of a PDT system with a hypoxia-responsive drug delivery system could be promising for enhanced anticancer therapy. Herein, we report an innovative conjugated polymer-based nanocarrier capable of light-triggered ROS generation and subsequently hypoxia-responsive anticancer drug release (**Figure 1**). This formulation (designated DOX/CP-NI NPs) comprises of three components: ROS-generating and hypoxia-sensitive 2-nitroimidazole-grafted conjugated polymer (CP-NI), polyvinyl alcohol (PVA)-based surface coatings, and encapsulated drug doxorubicin hydrochloride (DOX) (**Figure 1**a). Conjugated polymers, with highly light harvesting and emitting, are being actively investigated in sensing, imaging, and medical therapeutics.[12] We synthesized a new multifunctional CP with dithiophene-benzotriazole[13] moiety that can be utilized as a visible/near-infrared (Vis/NIR) light-activated ROS generation source, and dithiophene-thienopyrazine[14] moiety as NIR imaging agent. In order to achieve hypoxia-responsive transduction, this CP was further grafted with 2-nitroimidazole (NI), a hydrophobic component. NI can be converted to hydrophilic 2-aminoimidazoles under a hypoxic environment *via* a single-electron reduction catalyzed by a series of nitroreductases coupled to bioreducing agents, such as NADPH, a plentiful coenzyme in tissues.[15] The drug carrier based on NI-grafted conjugated polymer (CP-NI) is expected to be bioreduced under hypoxic conditions, leading to disassembly of drug carrier.

After intravenous (i.v.) injection, the DOX/CP-NI NPs could be accumulated into the tumor sites by the enhanced permeability and retention (EPR) effect[16], and then internalized into the cells through endocytosis (**Figure 1**b). Upon light irradiation, these NPs are able to produce $^1O_2$ for disruption of the endo-/lysosomal membrane and induction of cell apoptosis.[17] Meanwhile, the dissolved oxygen can be rapidly consumed due to the generation of $^1O_2$, which leads to a local hypoxic environment. Therefore, NI groups on the CP-NI could be reduced to hydrophilic 2-aminoimidazoles under bioreductive conditions in

cells, promoting the dissociation of DOX/CP-NI, and subsequent release of cargo. The released DOX could accumulate into the nuclei to induce DNA damage-mediated cytotoxicity[18], which combines with the apoptosis effect of PDT for an enhanced synergistic antitumor activity.

To substantiate our design, we first synthesized ROS-generating and hypoxia-sensitive CP-NI by alternating copolymerization of fluorene (a high-efficient blue emitting unit), dithiophene-benzotriazole (an excellent sensitizer for the generation of $^1O_2$[13]), and dithiophene-thienopyrazine (a unit to effectively shift emission maximum to NIR wavelengths[14])-containing monomers *via* the Suzuki cross-coupling reaction. Then, the branched chains were further modified with NI by the nucleophilic substitution reaction (Figure S1). The obtained CP-NI was a hydrophobic polymer, which was utilized to encapsulate DOX through a double-emulsion-based solvent evaporation/extraction method[19] (**Figure 1**a). Under a hypoxic condition, the NI group on the branched chains is expected to be bioreduced and alter its hydrophobicity, which promotes the disassembly of DOX/CP-NI NPs.[20] The transmission electron microscopy (TEM) image of DOX/CP-NI NPs clearly revealed its core-shell structure (inset of **Figure 2**a). The average hydrodynamic diameter of the DOX/CP-NI NPs was determined as 118 nm by dynamic light scattering (DLS) (**Figure 2**a), which did not change for at least 7 days (Figure S4a), indicating the long-term stability of NPs in the culture media. The DOX loading capacity was measured to be 20.8% (wt/wt). The UV/Vis absorption spectrum of DOX/CP-NI NPs in aqueous suspension displayed two absorption bands at 500 and 600 nm, respectively (**Figure 2**b), suggesting the NPs had a broad absorption spectrum, and both visible and NIR light were able to induce the production of ROS. The maximum emission wavelength of CP-NI was 740 nm (excited at 488 nm) (Figure S5a), indicating that the NPs have NIR emission, which is suitable for *in vivo* imaging. Furthermore, there is no significant photobleaching of NPs within the 20 min irradiation period and only 13.3% decrease in fluorescence intensity under continuous illumination for 60 min (Figure S5b).

Next, the ROS generation induced by CP-NI or DOX/CP-NI NPs upon light irradiation was evaluated using 1,3-diphenylisobenzofuran (DPBF), a typical singlet oxygen ($^1O_2$) indicator, whose absorption is irreversibly quenched by $^1O_2$[21] The absorption intensity of DPBF in CP-NI NPs solution decreased quickly upon the irradiation with visible light (λ=532 nm) within 30 s, indicating that $^1O_2$ was efficiently produced by CP-NI. In addition, using longer wavelength excitation (λ=635 nm) can also generate $^1O_2$ rapidly (Figure S6). 2',7'-Dichlorofluorescin diacetate (DCFH-DA), as a ROS indicator utilized for assessment of ROS production, which can be rapidly oxidized by ROS to a green fluorescent molecule (dichlorofluorescein, DCF).[22] Upon the irradiation of CP-NI or DOX/CP-NI NP for 6 min, a strong fluorescence of DCF was detected at 525 nm, whereas the fluorescence intensity of the control groups without the NPs remained at the original level (**Figure 2**c). Meanwhile, a faster ROS production rate was achieved with increase in power density. While adding vitamin C (VC, a ROS scavenger), the fluorescence was significantly inhibited, further confirming DOX/CP-NI-mediated ROS generation upon light irradiation.

To evaluate DOX/CP-NI NPs-mediated hypoxia generation *in vitro*, the NPs were incubated with PBS buffer containing NADPH, cytochrome *c* reductase, and DPBF (as $^1O_2$

scavenger).[15b] The oxygen consumption, caused by the conversion of oxygen to ROS induced by CP-NI NPs with light irradiation, was measured using an oxygen-sensitive phosphorescent molecular probe[23]. Upon light irradiation, the samples of CP-NI or DOX/CP-NI NPs had a lower oxygen concentration compared with the other control samples. Of note, a faster oxygen consumption rate was achieved with increase in power density (**Figure 2**d). In this light-triggered hypoxic environment, the nitro groups on the side-chains of CP-NI were effectively reduced by electrons from NADPH catalyzed by the reductase, resulting in accelerating dissociation of DOX/CP-NI NPs. The corresponding evolution of morphology and size changes were clearly observed through TEM imaging and DLS (**Figure 2**e, **2**f, and S4b). The NPs remarkably swelled after 5 min irradiation, and totally disassembled after 24h.

To evaluate the light-triggered release behavior of DOX from DOX/CP-NI NPs, the NPs were irradiated with light at a power density of 0.1 W cm^{-2} for 20 min before monitoring DOX release. After 48h, approximately 60 % of DOX was released at pH 7.4 due to the dissociation of the NPs, whereas only a small amount of DOX was released from the NPs in PBS solution without irradiation (**Figure 2**g). To validate if the DOX release speed directly corresponds to the reduction of NI groups in a low oxygen level rather than decreased pH level, the DOX release kinetics at pH 5.4 solution were investigated. The results showed that there was insignificant DOX release from the NPs incubated at pH 5.4 without light irradiation, confirming the NPs were stable under an acidic condition. It is especially worth noting that a higher cumulative DOX release at pH 5.4 was achieved compared to that at pH 7.4 after irradiation with light, suggesting these NPs may potentially have better performance in the acidic endosomal environment[24]. Moreover, the DOX release profile of DOX/CP-NI NPs presented a pulsatile pattern when they were alternatively exposed to light and kept in dark every 20 min for several cycles (**Figure 2**h). Collectively, it was demonstrated that the disassembly of DOX/CP-NI NPs underwent a light-activated and hypoxia-dependent process.

To clarify CP-NI NPs-mediated ROS generation and the induced local hypoxic environment in tumor cells, the CP-NI NPs-loaded human cervical cancer (HeLa) cells were detected using ROS/hypoxia detection probes with or without light treatments, respectively. ROS-induced and hypoxia-induced samples were used as the positive controls, and the untreated sample as a negative control. As shown in **Figure 3**a, the stronger fluorescence of the ROS production (green color) and hypoxia generation (magenta color) upon irradiation were observed by the confocal laser scanning microscopy (CLSM), indicating a high level of ROS production and a light-induced hypoxic environment inside cells. Furthermore, the CP-NI NPs-mediated ROS generation and oxygen consumption were quantitatively measured by the flow cytometry assays (**Figure 3**b). Under irradiation, the rates of ROS production and oxygen consumption of DOX/CP-NI-treated cells were 68.3% and 41.2%, respectively.

We next investigated the release of DOX in the cells triggered by light-induced hypoxic environment. HeLa cells were incubated with DOX/CP-NI NPs for 2 h in dark and then irradiated with light at a power density of 0.1 W cm^{-2} for 20 min. Afterwards, the cells were incubated with fresh culture medium for an additional 2 or 4h, followed by the observation *via* CLSM. DOX fluorescence was observed intracellularly during the first 2h of the cellular

uptake of DOX/CP-NI NPs (Figure S7 and **Figure 4**a). Notably, DOX/CP-NI NPs presented a concomitant increase of DOX fluorescence intensity in the nuclei with an additional 2 h and 4 h incubation. The broader red fluorescence and less green fluorescence suggested the effective endo-/lysosomal escape of DOX/CP-NI NPs due to the light-triggered ROS generation and subsequent damage of the endo-/lysosomal membrane.[17] Meanwhile, oxygen was rapidly consumed to produce a local hypoxic condition, which resulted in the dissociation of DOX/CP-NI NPs and subsequent release of the DOX that specifically accumulated into the nuclei, as evidenced by the magenta fluorescent signals. To further demonstrate DOX/CP-NI NPs-mediated hypoxia-responsive DOX release, HeLa cells were incubated with DOX/CP-NI NPs in dark or in the presence of VC for inhibiting the ROS generation. As shown in **Figure 4**a, the cells incubated both in dark and with VC showed insignificant DOX fluorescent signals in the nuclei, and most of the DOX/CP-NI NPs were located in the endosomes. Collectively, these results substantiated that the light-activated hypoxic condition could promote the release of DOX in the cells.

Furthermore, the Annexin V-FITC/PI apoptosis detection assay[25] was performed to compare the apoptosis-inducing capabilities of DOX/CP-NI NPs before and after irradiation. The early and late apoptosis of HeLa cells were monitored by CLSM (Figure S8). After irradiation with light, DOX/CP-NI NPs-treated HeLa cells displayed a stronger fluorescence with apoptotic characteristics. In addition, the quantitative results by flow cytometry verified the optimal synergistic apoptotic efficacy of DOX/CP-NI NPs-mediated PDT and hypoxia-responsive DOX release (**Figure 4**b). DOX/CP-NI NPs showed the highest total apoptotic ratio of 58.0% (a sum of the early apoptotic ratio of 32.1% and the late apoptotic ratio of 25.9%) and the lowest viability of 35.6% compared with other samples.

The *in vitro* cytotoxicity of DOX/CP-NI NPs against HeLa cells was evaluated by using 3-(4,5-dimethylthiazol-2-yl)-2,5-diphenyltetrazolium bromide (MTT) assay[26]. DOX/CP-NI NPs irradiated with 532 nm light (0.1 W cm^{-2}, 20 min) exhibited significantly enhanced cytotoxicity compared with the groups with CP-NI NPs in dark, DOX/CP-NI NPs in dark, CP-NI NPs in light, and DOX/CP-NI NPs in light at all studied DOX or CP-NI concentrations (Figure S9). Notably, the cytotoxicity increased along with the concentration of DOX with a half lethal dose (IC_{50}) of 1.6 μg mL^{-1} at incubation time of 24 h. Moreover, treatment with only light or CP-NI NPs and DOX/CP-NI NPs without light did not result in a significant decrease in the cell viability (**Figure 4**c), indicating the negligible toxicity of both types of the NPs to HeLa cells. In contrast, CP-NI NPs under irradiation showed significant cytotoxicity to the cancer cells, which can be attributed to the production of ROS in the cells. In addition, incubation of the cells with DOX/CP-NI NPs at the same irradiation condition led to higher cytotoxicity than that of the cells treated with free DOX, indicating an enhanced potency could be achieved using a combination of photodynamic therapy and stimuli-responsive chemotherapy.

To explore the *in vivo* NIR imaging capability of the CP-NI, DOX/CP-NI NPs were administrated intravenously into the HeLa tumor-bearing mice *via* tail vein. The blood circulation profile of DOX/CP-NI NPs (Figure S10) gave half-life ($T_{1/2}$) of 4.0 h, which indicating a long persistence of the NPs in bloodstream, which could be attributed to the presence of PVA shell[27]. And as shown in **Figure 5**a, a strong fluorescence signal of CP-NI

was detected at the tumor site 6 h post-injection. As time extended, a higher CP-NI signal in tumor than in the normal tissues after administration for 24h, suggesting that the DOX/CP-NI NPs could be accumulated into the tumor sites. Upon light irradiation (maximum excitation wavelength: 532 nm, 0.28 W cm^{-2}) for 5 min, a decreased fluorescence intensity was found at the tumor site at 48 h post administration, and followed the tumor and normal tissues were harvested for *ex vivo* imaging. The relative fluorescence signal biodistribution of DOX/CP-NI NPs can be found at the tumor and other normal organs (**Figure 5**b). The results were confirmed by the quantitative region-of-interest (ROI) analysis (**Figure 5**c). The fluorescence intensity biodistribution percentage of CP-NI was 2.8%, 34.7%, 2.7%, 27.8%, 11.7% and 20.3% of at heart, liver, spleen, lung, kidney, and tumor tissue, respectively. These results indicated that CP-NI has potential to be exploited as an efficient drug-delivery system for imaging-guided therapeutics[28].

To assess the *in vivo* efficacy of DOX/CP-NI NPs for antitumor treatment, the HeLa tumor-bearing mice were exposed to treatment with different samples, including the saline, light, DOX/CP-NI NPs, CP-NI NPs with light, or DOX/CP-NI NPs with light. As shown in **Figure 5**d and **5**e, the growth of the tumor was completely inhibited in the group associated with the light-activated hypoxia-triggered DOX release, compared with those of the saline, light-only or DOX/CP-NI NPs-only groups. The tumor treated with CP-NI NPs upon irradiation also showed a moderate tumor inhibition capability than those of control groups due to generation of ROS by CP-NI NPs with irradiation. However, it is notable that DOX/CP-NI NPs with light irradiation brought about the strongest effect on suppressing the tumor growth, which validated that hypoxia-responsive DOX release of DOX/CP-NI NPs activated by light enabled the reinforcement on the anticancer efficacy. The body weight of mice treated with different samples shown no noticeable change during the treatment (Figure S11). The hematoxylin and eosin (HE) and the terminal deoxynucleotidyl transferase dUTP nick end labeling (TUNEL) staining assays were also performed to evaluate the treatment efficacy with different treatments, respectively (**Figure 5**f). The images of HE-stained tumor tissue presented prominent necrosis of tumor cells treated by DOX/CP-NI NPs with light. The images obtained from the TUNEL staining showed the highest level of cell apoptosis in the tumor tissue of the mice receiving DOX/CP-NI NPs with light. Furthermore, no obvious pathological abnormalities were observed in normal organs (Figure S12). Additionally, considering the efficient penetration depth of the irradiation, a 635 nm laser was also employed to activate the DOX/CP-NI NPs for *in vivo* antitumor treatment (Figure S13), and the results also exhibited highly efficient antitumor potency.

In conclusion, we reported a novel drug delivery platform, for the first time, utilizing light-activated hypoxia-responsive modality, which combines both photodynamic therapy and chemotherapy for enhanced treatment efficacy. Such conjugated polymer-based delivery system is able to efficiently produce ROS and induce hypoxia to promote release of its cargoes inside cells both *in vitro* and *in vivo*. This strategy provides an innovative design guideline for stimuli-responsive drug delivery systems[29], which can undergo a series of programmed multiple triggers: the effect of one primary trigger activates the other trigger(s) for achieving synergistic treatment efficacy[30].

Supplementary Material

Refer to Web version on PubMed Central for supplementary material.

Acknowledgements

C. Qian, J. Yu, and Y. Chen contributed equally to this work. This work was supported by the grants from NC TraCS, NIH's Clinical and Translational Science Awards (CTSA, NIH Grant No. 1UL1TR001111) at UNC-CH, National Natural Science Foundation of China (No. 21174060), and Program for Changjiang Scholars and Innovative Research Team in University (No. IRT1252). The authors acknowledge the use of the Analytical Instrumentation Facility (AIF) at NC State, which is supported by the State of North Carolina and the National Science Foundation (NSF). The authors greatly thank the China Scholarship Council for financially supporting C. Qian's foreign research and life.

References

1. a Dolmans DE, Fukumura D, Jain RK. Nat. Rev. Cancer. 2003; 3:380. [PubMed: 12724736] b Triesscheijn M, Baas P, Schellens JH, Stewart FA. Oncologist. 2006; 11:1034. [PubMed: 17030646] c Idris NM, Gnanasammandhan MK, Zhang J, Ho PC, Mahendran R, Zhang Y. Nat. Med. 2012; 18:1580. [PubMed: 22983397]
2. a Dougherty TJ, Gomer CJ, Henderson BW, Jori G, Kessel D, Korbelik M, Moan J, Peng Q. J. Natl. Cancer Inst. 1998; 90:889. [PubMed: 9637138] b Niedre M, Patterson MS, Wilson BC. Photochem. photobiol. 2002; 75:382. [PubMed: 12003128]
3. Lovell JF, Liu TW, Chen J, Zheng G. Chem. Rev. 2010; 110:2839. [PubMed: 20104890]
4. a Cheng L, Wang C, Feng L, Yang K, Liu Z. Chem. Rev. 2014; 114:10869. [PubMed: 25260098] b Kerativitayanan P, Carrow JK, Gaharwar AK. Adv. Healthc. Mater. 2015c Ariga K, Kawakami K, Ebara M, Kotsuchibashi Y, Ji Q, Hill JP. New J. Chem. 2014; 38:5149.
5. a Nomoto T, Fukushima S, Kumagai M, Machitani K, Arnida, Matsumoto Y, Oba M, Miyata K, Osada K, Nishiyama N, Kataoka K. Nat. Commun. 2014; 5:3545. [PubMed: 24694458] b Zhu X, Xu Y, Solis LM, Tao W, Wang L, Behrens C, Xu X, Zhao L, Liu D, Wu J. Proc. Natl. Acad. Sci. U. S. A. 2015; 112:7779. [PubMed: 26056316] c Lin Q, Bao C, Yang Y, Liang Q, Zhang D, Cheng S, Zhu L. Adv. Mater. 2013; 25:1981. [PubMed: 23401259] d Perche F, Biswas S, Wang T, Zhu L, Torchilin VP. Angew. Chem. Int. Ed. Engl. 2014; 53:3362. [PubMed: 24554550]
6. Cheng Y, Meyers JD, Broome A-M, Kenney ME, Basilion JP, Burda C. J. Am. Chem. Soc. 2011; 133:2583. [PubMed: 21294543]
7. a Wang C, Cheng L, Liu Y, Wang X, Ma X, Deng Z, Li Y, Liu Z. Adv. Funct. Mater. 2013; 23:3077.b Rieffel J, Chen F, Kim J, Chen G, Shao W, Shao S, Chitgupi U, Hernandez R, Graves SA, Nickles RJ. Adv. Mater. 2015; 27:1785. [PubMed: 25640213] c Liu Y, Bu W, Cheng C, Zuo C, Xiao Q, Sun Y, Ni D, Zhang C, Liu J, Shi J. Angew. Chem. Int. Ed. Engl. 2015; 54:8105. [PubMed: 26012928]
8. a Huang P, Lin J, Wang X, Wang Z, Zhang C, He M, Wang K, Chen F, Li Z, Shen G, Cui D, Chen X. Adv. Mater. 2012; 24:5104. [PubMed: 22718562] b Nakanishi W, Minami K, Shrestha LK, Ji Q, Hill JP, Ariga K. Nano Today. 2014; 9:378.
9. a Tu HL, Lin YS, Lin HY, Hung Y, Lo LW, Chen YF, Mou CY. Adv. Mater. 2009; 21:172.b Chen F, Hong H, Goel S, Graves SA, Orbay H, Ehlerding EB, Shi S, Theuer CP, Nickles RJ, Cai W. ACS nano. 2015; 9:3926. [PubMed: 25843647] c Coll C, Bernardos A, Martínez-Máñez R, Sancenón F. Acc. Chem. Res. 2013; 46:339. [PubMed: 23214509]
10. a Henderson BW, Fingar VH. Cancer Res. 1987; 47:3110. [PubMed: 3581062] b Mitchell JB, McPherson S, DeGraff W, Gamson J, Zabell A, Russo A. Cancer Res. 1985; 45:2008. [PubMed: 3157442]
11. Wang W, Moriyama LT, Bagnato VS. Laser Phys. Lett. 2013; 10:023001.
12. a Sun B, Sun M-J, Gu Z, Shen Q-D, Jiang S-J, Xu Y, Wang Y. Macromolecules. 2010; 43:10348.b Traina CA, Bakus RC II, Bazan GC. J. Am. Chem. Soc. 2011; 133:12600. [PubMed: 21751809] c Ahmed E, Morton SW, Hammond PT, Swager TM. Adv. Mater. 2013; 25:4504. [PubMed: 23794490] d Yuan Y, Liu J, Liu B. Angew. Chem. Int. Ed. Engl. 2014; 53:7163. [PubMed:

24861823] e Yuan Y, Zhang CJ, Liu B. Angew. Chem. Int. Ed. Engl. 2015; 54:11419. [PubMed: 26094980] f Feng L, Liu L, Lv F, Bazan GC, Wang S. Adv. Mater. 2014; 26:392.

13. Patel DG, Feng F, Ohnishi YY, Abboud KA, Hirata S, Schanze KS, Reynolds JR. J. Am. Chem. Soc. 2012; 134:2599. [PubMed: 22296041]
14. Yu JC, Chen YL, Zhang YQ, Yao XK, Qian CG, Huang J, Zhu S, Jiang XQ, Shen QD, Gu Z. Chem. Commun. 2014; 50:4699.
15. a Nunn A, Linder K, Strauss HW. Eur. J. Nucl. Med. 1995; 22:265. [PubMed: 7789400] b Yu J, Zhang Y, Ye Y, DiSanto R, Sun W, Ranson D, Ligler FS, Buse JB, Gu Z. Proc. Natl. Acad. Sci. U. S. A. 2015; 112:8260. [PubMed: 26100900]
16. a Peer D, Karp JM, Hong S, Farokhzad OC, Margalit R, Langer R. Nat. Nanotechnol. 2007; 2:751. [PubMed: 18654426] b Farokhzad OC, Langer R. ACS nano. 2009; 3:16. [PubMed: 19206243]
17. Hogset A, Prasmickaite L, Selbo PK, Hellum M, Engesaeter BO, Bonsted A, Berg K. Adv. Drug Deliv. Rev. 2004; 56:95. [PubMed: 14706447]
18. Tewey KM, Rowe TC, Yang L, Halligan BD, Liu LF. Science. 1984; 226:466. [PubMed: 6093249]
19. a Gu Z, Aimetti AA, Wang Q, Dang TT, Zhang Y, Veiseh O, Cheng H, Langer RS, Anderson DG. ACS nano. 2013; 7:4194. [PubMed: 23638642] b Di J, Yao S, Ye Y, Cui Z, Yu J, Ghosh TK, Zhu Y, Gu Z. ACS nano. 2015; 9:9407. [PubMed: 26258579]
20. Zhu C, Liu L, Yang Q, Lv F, Wang S. Chem. Rev. 2012; 112:4687. [PubMed: 22670807]
21. Zhao Z, Han Y, Lin C, Hu D, Wang F, Chen X, Chen Z, Zheng N. Chem. Asian. J. 2012; 7:830. [PubMed: 22279027]
22. Shim MS, Xia Y. Angew. Chem. Int. Ed. Engl. 2013; 52:6926. [PubMed: 23716349]
23. a Will Y, Hynes J, Ogurtsov VI, Papkovsky DB. Nat. Protoc. 2006; 1:2563. [PubMed: 17406510] b Fercher A, Borisov SM, Zhdanov AV, Klimant I, Papkovsky DB. ACS nano. 2011; 5:5499. [PubMed: 21671589]
24. a Tannock IF, Rotin D. Cancer Res. 1989; 49:4373. [PubMed: 2545340] b Yang XZ, Du XJ, Liu Y, Zhu YH, Liu YZ, Li YP, Wang J. Adv.Mater. 2014; 26:931. [PubMed: 24338636]
25. a Vermes I, Haanen C, Steffens-Nakken H, Reutellingsperger C. J. Immunol. Methods. 1995; 184:39. [PubMed: 7622868] b Kim Y, Lobatto ME, Kawahara T, Chung BL, Mieszawska AJ, Sanchez-Gaytan BL, Fay F, Senders ML, Calcagno C, Becraft J. Proc. Natil.Acad. Sci. U. S. A. 2014; 111:1078.
26. Hu Q, Sun W, Qian C, Wang C, Bomba HN, Gu Z. Adv. Mater. 2015; 27:7043. [PubMed: 26416431]
27. Burczak K, Gamian E, Kochman A. Biomaterials. 1996; 17:2351. [PubMed: 8982475]
28. a Cai W, Chen X. J. Nucl. Med. 2008; 49(Suppl 2):113S. [PubMed: 18523069] b Zhang RP, Fan QL, Yang M, Cheng K, Lu XM, Zhang L, Huang W, Cheng Z. Adv. Mater. 2015; 27:5063. [PubMed: 26222210]
29. Lu Y, Sun W, Gu Z, Control J. Release. 2014; 194:1.
30. a Mitragotri S, Anderson DG, Chen X, Chow EK, Ho D, Kabanov AV, Karp JM, Kataoka K, Mirkin CA, Petrosko SH. ACS nano. 2015; 9:6644. [PubMed: 26115196] b Pacardo DB, Ligler FS, Gu Z. Nanoscale. 2015; 7:3381. [PubMed: 25631684]

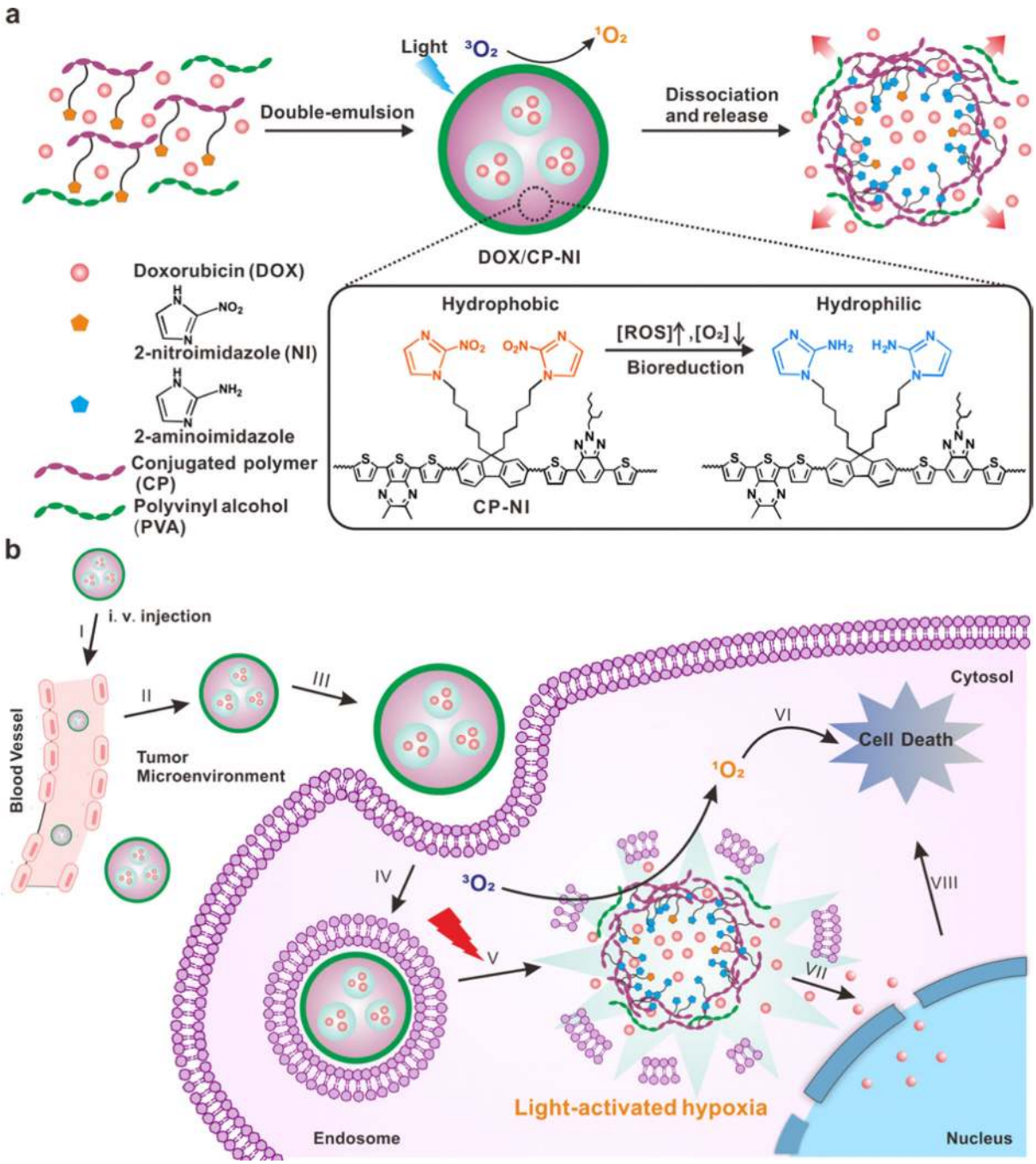

Figure 1.

Schematic of the light-activated hypoxia-responsive drug delivery system. a) Formation and mechanism of DOX/CP-NI NPs. b) Schematic of DOX/CP-NI NPs for ROS generation and induced a local hypoxic environment capable of hypoxia-responsive release DOX into cell nuclei for enhanced synergistic anticancer efficacy.

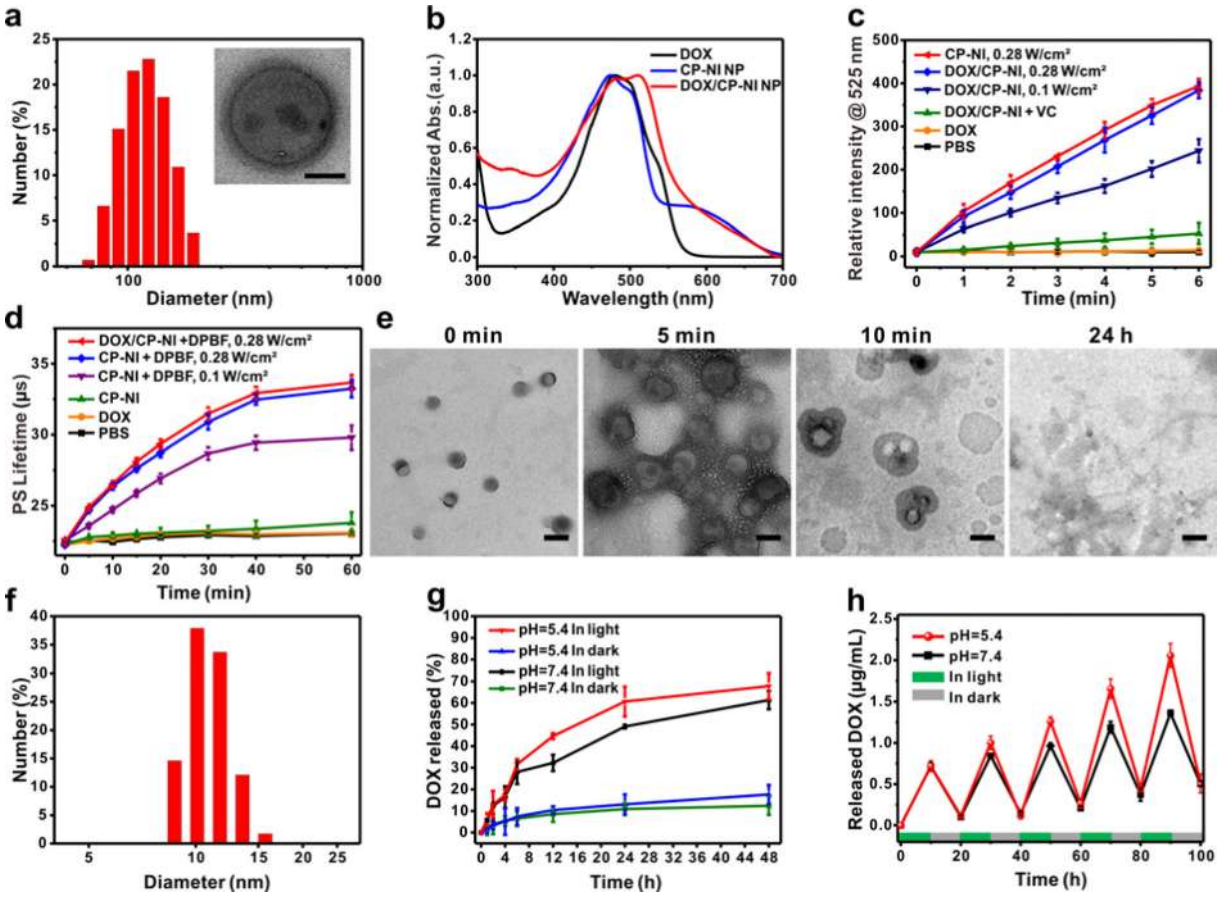

Figure 2.

Characterization and *in vitro* light-activated hypoxia-responsive DOX release of DOX/CP-NI NPs. a) Hydrodynamic size distribution and TEM image (inset) of DOX/CP-NI NPs. Scale bar is 50 nm. b) Normalized UV/Vis absorption spectra of DOX, CP-NI NPs, and DOX/CP-NI NPs. c) Fluorescence intensity of DCF at 525 nm in PBS, with DOX in PBS, with DOX/CP-NI NPs in PBS, and with CP-NI NPs in PBS after irradiation with light for different time. VC was the ROS scavenger. d) Phosphorescence (PS) lifetime profile over exposure time in PBS, with DOX in PBS, with CP-NI NPs in PBS, and with DOX/CP-NI NPs in PBS containing an oxygen concentration molecule probe. DPBF as the $^1O_2$ scavenger. e) TEM images of DOX/CP-NI NPs for different time after 5 min light irradiation. Scale bars are 200 nm. f) Size distribution of DOX/CP-NI NPs at 24h after 5 min light irradiation treatment. g) *In vitro* release of DOX from DOX/CP-NI NPs in PBS in dark or in light and with different pH at 37 °C. h) Pulsatile release profile of DOX/CP-NI NPs at different pH presents the rate of DOX release both in dark and in light. Error bars indicate SD (n = 3).

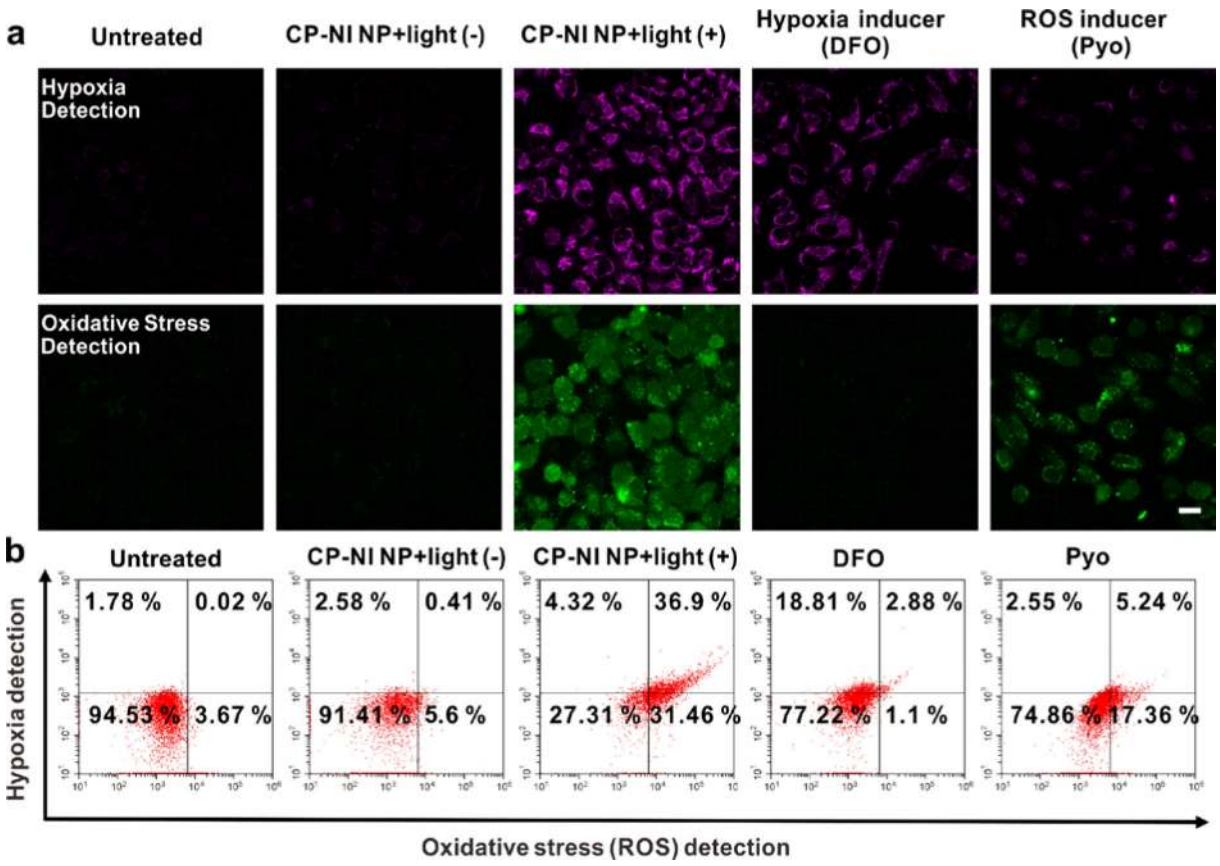

Figure 3.

CP-NI NPs-mediated generation of ROS and hypoxic environment in HeLa cells. a) Confocal fluorescence images of HeLa cells with ROS/hypoxia detection probes in different treatments: untreated, CP-NI NPs without light, CP-NI NPs with light, and positive control groups (ROS-induced and hypoxia-induced), respectively. Scale bar is 50 μm. b) Flow cytometry analysis of ROS production and hypoxia environment in HeLa cells with different treatments.

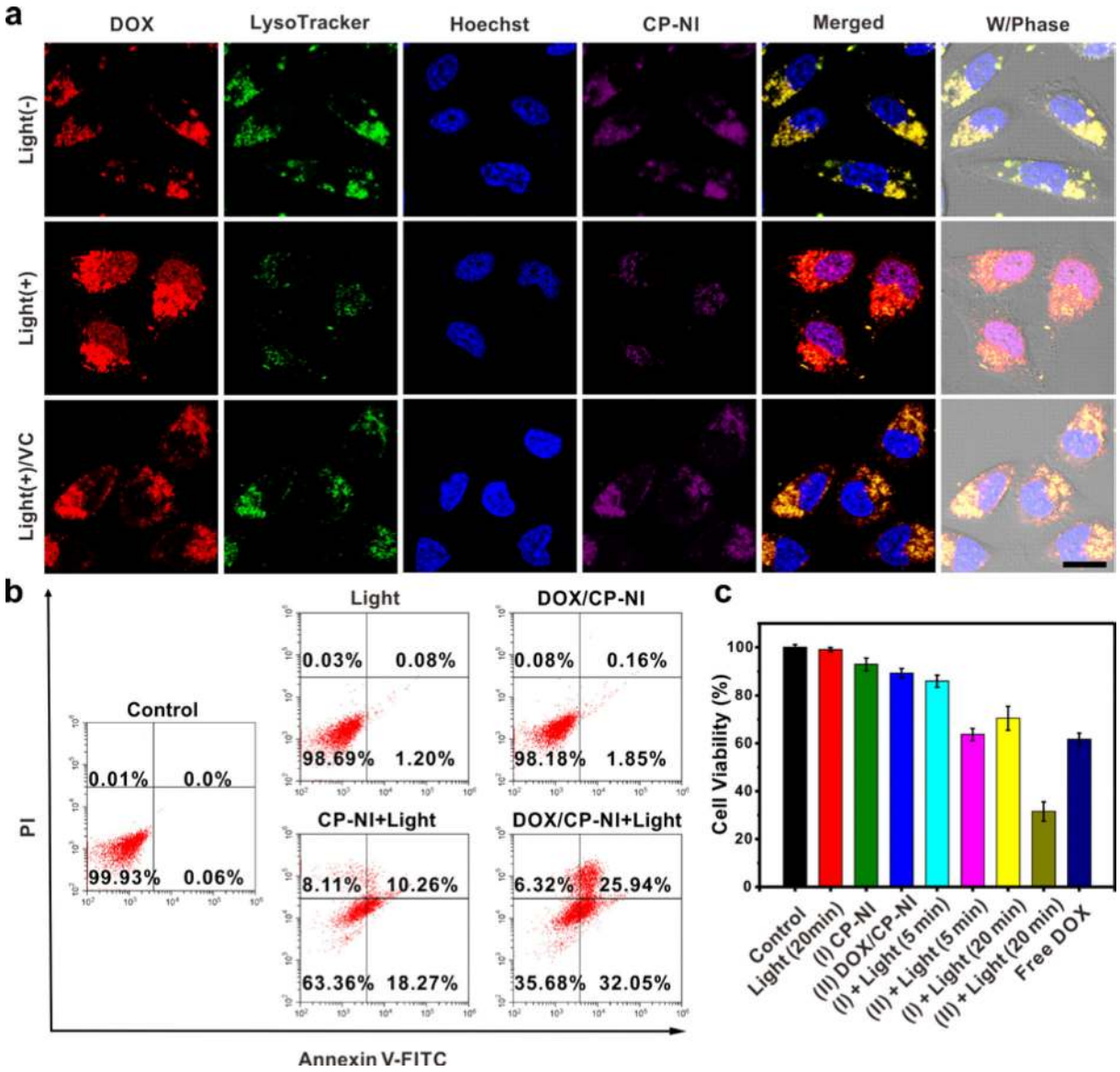

Figure 4.

Intracellular DOX/CP-NI NPs-mediated hypoxia-triggered DOX release. a) Intracellular delivery of DOX/CP-NI NPs on HeLa cells treated with different formulations observed by CLSM, including without light, with light, and with the ROS scavenger VC. The endosomes and lysosomes were stained by LysoTracker Green, and the nuclei were stained by Hoechst 33342. Merged (DOX/ LysoTracker/ Hoechst). Scale bar is 20 μm. b) Flow cytometry analysis of HeLa cell apoptosis induced by different formulations for 12 h using the Annexin V-FITC/PI staining. c) *In vitro* cytotoxicity of HeLa cells incubated for 24 h with free DOX, and CP-NI NPs and DOX/CP-NI NPs without or with irradiation (5 or 20 min). Control sample was without any treatment. Error bars indicate SD (n = 3).

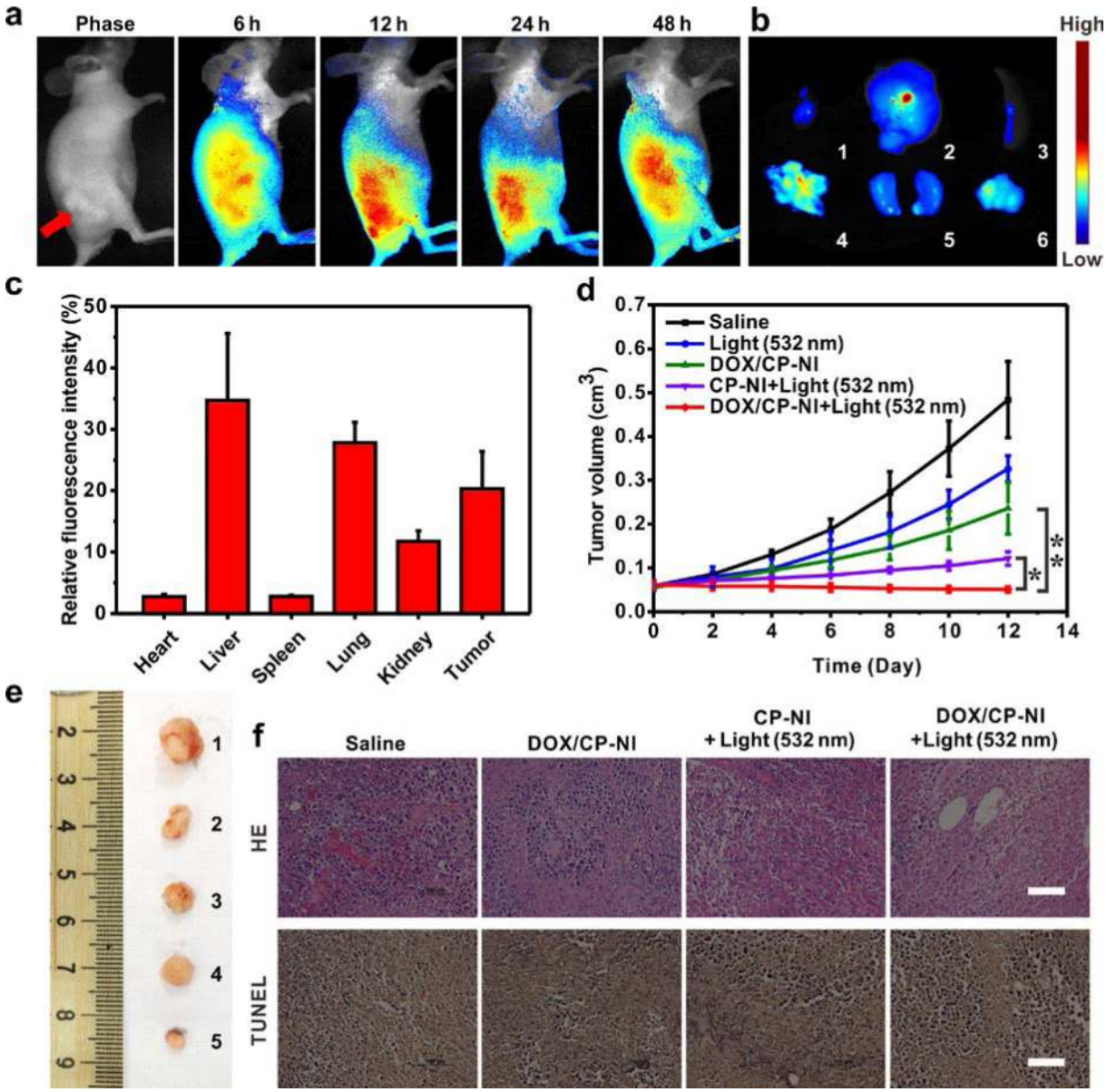

Figure 5.

In vivo fluorescence imaging and antitumor efficacy of DOX/CP-NI NPs. a) *In vivo* fluorescence images of the HeLa tumor-bearing nude mice at 6, 12, 24, and 48 h after intravenous injection of DOX/CP-NI NPs. Arrows indicate the sites of tumors. b) *Ex vivo* fluorescence imaging of the normal organs and tumor collected from the mice at 48 h after administration (1: heart, 2: liver, 3: spleen, 4: lung, 5: kidney, 6: tumor). c) The quantitative region-of-interest (ROI) analysis of fluorescent signals of the tumor and normal organs. Error bars indicate SD (n = 3). d) The HeLa tumor growth curves upon different treatments (2.0 mg kg^{-1} DOX, 3.6 mg kg^{-1} CP-NI). $^{*}P < 0.05$, $^{**}P < 0.01$ (two-tailed Student's *t*-test). Error bars indicate SD (n = 5). e) Representative images of the HeLa tumors after treatment with different samples at day 12 (from top to bottom, 1: saline, 2: light, 3: CP-NI NPs, 4: CP-NI NPs with light, 5: DOX/CP-NI NPs with light). f) Histological observation of the

tumor tissues stained with H&E after treatment with different samples, and detection of apoptosis in the tumor tissues after treatment with the TUNEL staining assay. Scale bars are 100 μm.